

Thermodynamic properties and thermal correlation lengths of a Hubbard model with bond-charge interaction

Andreas Kemper* and Andreas Schadschneider†

Institute for Theoretical Physics, University of Cologne, 50937 Köln, Germany

(Dated: November 5, 2018)

We investigate the thermodynamics of a one-dimensional Hubbard model with bond-charge interaction X using the transfer matrix renormalization group method (TMRG). Numerical results for various quantities like spin and charge susceptibilities, particle densities, specific heat and thermal correlation lengths are presented and discussed. We compare our data also to results for the exactly solvable case $X/t = 1$ as well as to bosonisation results for weak coupling $X/t \ll 1$, which shows excellent agreement. We confirm the existence of a Tomonaga-Luttinger and a Luther-Emery liquid phase, in agreement with previous studies at zero temperature. Thermal singlet-pair correlation lengths are shown to dominate density and spin correlations for finite temperatures in certain parameter regimes.

PACS numbers: 71.10.Fd, 71.27.+a, 5.10.Cc, 5.30.-d, 5.70.-a

I. INTRODUCTION

The Coulomb interaction between electrons in a solid does not only lead to diagonal terms like the Hubbard interaction. It is also responsible for other non-diagonal terms that are often neglected since the corresponding coupling constants are assumed to be small. However, this is not always true. Hirsch (see e.g. refs. 1,2 and references therein) has argued that especially the bond-charge interaction X may be responsible for interesting physics based on the breaking of particle-hole symmetry.

In refs. 3,4,5 it has been shown within a BCS-type analysis that the bond-charge interaction can induce an effective attraction between particles at densities $n > 1$, which can even lead to the formation of Cooper pairs and superconductivity. More evidence for this scenario has been obtained in analytical^{6,7,8,9,10,11,12} and numerical^{13,14,15,16} studies of one-dimensional variants and an effective model for CuO₂ planes¹⁷. Other materials where bond-charge interaction might play an important role are polyacetylene (see ref. 18 and references therein) and the Bechgaard salts¹⁹.

The Bechgaard salts show a rich phase diagram as temperature and pressure are varied²⁰. At temperatures not too low these materials can be regarded as quasi one-dimensional. In order to elucidate the relevance of bond-charge interactions it is therefore interesting to study thermodynamic properties of one-dimensional generalized Hubbard models with bond-charge interactions. This has been done in ref. 21 for the integrable case $t = X$ where t is the single-particle hopping matrix. Here the Hamiltonian simplifies considerably since the number of doubly-occupied sites is conserved. This allows for an exact solution for the complete spectrum^{22,23,24} which has then been used for the calculation of the thermodynamics in ref. 21. However, it should be noted that the Hamiltonian at $t = X$ has particle-hole symmetry such that the physics is different from Hirsch's scenario. We therefore investigate here the thermodynamics away from the point $t = X$. Since no exact solution is available one

has to rely on numerical methods. Here we employ the transfer matrix DMRG (TMRG) algorithm.

The TMRG method was originally introduced by Nishino²⁵ to study two-dimensional classical models. An adaptation to thermodynamics of quantum systems was proposed by Xiang et. al^{26,27,28}, who used a Trotter-Suzuki decomposition^{29,30} to map the 1D quantum model to a 2D classical one. Thereby, various thermodynamic properties can be studied with high precision^{31,32,33}. Similar ideas have recently been applied to stochastic models^{34,35}.

The paper is organised as follows. In Sec. II we present the model and its known properties. In Sec. III the TMRG approach to the thermodynamics of one-dimensional quantum systems is explained. Especially we emphasize the extensions necessary due to the fermionic nature of the problem. Sec. IV contains our main results. We analyze not only thermodynamic quantities like specific heat and susceptibilities, but also correlation functions, expressed by thermal correlation lengths. Sec. V contains a summary and conclusions.

II. THE MODEL

The Hamiltonian of the one-dimensional bond-charge interaction model reads

$$\mathcal{H} = -t \sum_{\langle ij \rangle \sigma} c_{i\sigma}^\dagger c_{j\sigma} + X \sum_{\langle ij \rangle \sigma} c_{i\sigma}^\dagger c_{j\sigma} (n_{i\bar{\sigma}} + n_{j\bar{\sigma}}) - h \sum_i (n_{i\uparrow} - n_{i\downarrow}) - \mu \sum_i (n_{i\uparrow} + n_{i\downarrow}) \quad (1)$$

where $c_{i\sigma}^\dagger$ and $c_{i\sigma}$, respectively, are fermionic creation and annihilation operators of an up- or down-electron ($\sigma = \uparrow, \downarrow$) at site i . In eq. (1) the index $\langle ij \rangle$ denotes the summation over adjacent lattice sites, $n_{i\sigma} = c_{i\sigma}^\dagger c_{i\sigma}$ the number of particles with spin σ at site i and $\bar{\sigma}$ the opposite of spin σ . Obviously, the amplitude $t > 0$ is

modified by $X > 0$, which correlates the hopping process to the charge of opposite spins.

The bond-charge model (1) exhibits full SU(2) spin and U(1) charge symmetry. Under the particle-hole transformation

$$c_{j\sigma} \rightarrow (-1)^j c_{j\sigma}^\dagger \quad (2)$$

the Hamiltonian transforms (up to constants) into

$$\mathcal{H}(t, X, \mu, h) \rightarrow \mathcal{H}(t - 2X, -X, -\mu, -h), \quad (3)$$

Thus, we can restrict ourselves to the parameter region $0 \leq X/t \leq 1$, which is representative for the whole model. $0 \leq X/t \leq 0.5$ coincides with $X/t \leq 0$ such that for weak X an repulsive correlated hopping amplitude transforms into an attractive one for holes. $0.5 \leq X/t \leq 1$ conversely corresponds to $X/t \geq 1$.

Generically, two universality classes of critical liquid phases are found for such two-component systems at temperature $T = 0$. In a Tomonaga-Luttinger liquid (TLL) phase spin and charge excitations are gapless and all correlation functions decay algebraically. In contrast, a Luther-Emery liquid (LEL) has a gapped spectrum of spin excitations and criticality is only observed for charge excitations.

For $X/t \ll 1$ the bond-charge model (1) can be treated within the framework of bosonisation techniques and renormalisation methods⁷. It was found, that (1) corresponds to an effective Hubbard model with

$$U_{\text{eff}} = 8X \cos(k_F), \quad (4)$$

and effective hopping amplitude

$$t_{\text{eff}} = (1 - nX)t \quad (5)$$

where n is the filling and $k_F = n\pi/2$. Thus, two phases appear for $X \ll 1$ corresponding to the effective Hubbard model: a TLL regime (repulsive Hubbard interaction) below half filling ($n < 1$) and a superconducting LEL (attractive Hubbard interaction) for $n > 1$. It is a crucial question, if the range of applicability of the bosonisation approach holds (qualitatively) for $X \sim t$. At least we know, that the integrable case $X/t = 1$ contradicts with the bosonisation results.

For $X/t = 1$ the bond-charge model (1) shows an additional SU(2) pseudospin symmetry induced by the so-called η -pair operators³⁶

$$\begin{aligned} \eta^\dagger &= \sum_i c_{i\downarrow}^\dagger c_{i\uparrow}^\dagger, & \eta &= \sum_i c_{i\uparrow} c_{i\downarrow}, \\ \eta^z &= \frac{1}{2} \sum_i (1 - c_{i\uparrow}^\dagger c_{i\uparrow} - c_{i\downarrow}^\dagger c_{i\downarrow}), \end{aligned} \quad (6)$$

and is particle-hole invariant due to eq. (3). Apart from that, the number of double occupied sites $N_{\uparrow\downarrow} = \sum_i n_{i\uparrow} n_{i\downarrow}$ is also conserved²³.

In that case the model is solvable by mapping the Hamiltonian to free spinless fermions^{22,23}. One can observe the complete energy spectrum of \mathcal{H} and distinguish three different $T = 0$ phases. At intermediate fillings $0.5 < n < 1.5$ some of the ground states are of η -pairing type, which show ODLRO and hence are superconducting^{36,37} (see, however, ref. 38). For small fillings $n < 0.5$ the ground states are identical to those of the $U = \infty$ Hubbard model. Due to particle-hole symmetry of the model, a corresponding phase occurs for large fillings $n > 1.5$. The model exhibits no spin gap, thus all phases fall into the TLL universality class.

The knowledge of the complete energy spectrum can be used to calculate the partition function $Z = \text{tr} e^{-\beta\mathcal{H}}$ exactly²¹. This leads to the grand canonical potential

$$-\beta\phi = \ln(1 + e^{2\beta\mu}) + \frac{1}{\pi} \int_0^\pi \ln(1 + e^{-\beta(\epsilon_k - \mu^*)}) dk \quad (7)$$

with $\epsilon_k = -2t \cos k$ and the effective chemical potential

$$\mu^*(\mu, \beta, h) = \mu + \frac{1}{\beta} \ln \frac{2 \cosh \beta h}{1 + e^{2\beta\mu}}. \quad (8)$$

The potential ϕ can be used to calculate various thermodynamic properties of the model rigorously²¹.

For the non-integrable regime $0 < X/t < 1$ detailed numerical studies of ground state properties and correlation functions are available^{7,13,14,15}. It was shown that the model exhibits a spin gap for $0 < X/t \lesssim 0.75$ and sufficiently large fillings. Conversely, the spin gap closes for $X/t \gtrsim 0.75$ and TLL behaviour is found for all fillings n .

A focus of refs. 13,14 was set on various two-point correlation functions, such as density, spin, singlet and triplet pair correlations. It was found that pair correlations are dominant for the spin gap regime $0 < X \lesssim 0.75$. $X/t \approx 0.5$ was identified as a particular point where the spin gap and the dominance of superconducting correlations are maximal.

The present paper expands the $T = 0$ studies to finite temperatures $T > 0$. Apart from the investigation of susceptibilities and the specific heat, we particularly focus on thermal correlation functions, especially the possibility of dominant superconducting pair correlations at $T > 0$. For the numerical analysis we use the transfer matrix DMRG (TMRG) method, which has been shown to be highly precise for fermionic models^{32,33} without suffering from minus-sign problems etc. There it has also been demonstrated, that the asymptotic behaviour of various correlation functions in terms of *thermal correlation lengths* are accessible by the TMRG algorithm.

III. THE TMRG METHOD

The transfer matrix DMRG (TMRG) method, a variant of White's DMRG algorithm^{39,40}, has originally been introduced by Nishino to study two-dimensional classical

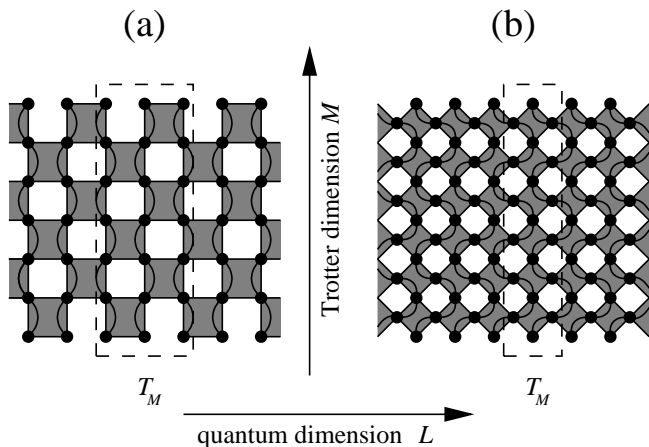


FIG. 1: Suzuki-Trotter decomposition of the partition function Z , leading to a classical two-dimensional lattice. The dots (\bullet) represent the lattice sites of classical spins, which interact by the shades plaquettes. In (a) the traditional mapping is plotted, cf. ref. 30. An alternative lattice is depicted in (b), which has additional auxiliary lattice points, cf. ref. 32. The quantum transfer matrix T_M is constructed column-wise.

systems²⁵. Xiang et. al applied the TMRG to the quantum transfer matrix (QTM) to study the thermodynamics of one-dimensional quantum systems^{26,27,28}. Since then it has been successfully used to study various spin and fermion systems^{31,32,33}.

A. Transfer matrix approach

The key idea of the TMRG is a Suzuki-Trotter decomposition^{29,30} of the partition function

$$Z = \text{tr} e^{-\beta\mathcal{H}} = \text{tr} (e^{-\epsilon\mathcal{H}_o} e^{-\epsilon\mathcal{H}_e})^M + O(\epsilon^2) \quad (9)$$

where $\epsilon = \beta/M$ is fixed and has to be chosen sufficiently small. The Hamiltonian \mathcal{H} consists of next-neighbour interactions $\mathcal{H} = \sum_i h_{i,i+1}$ and is split up into $\mathcal{H}_{o/e} = \sum_{o/e} h_{i,i+1}$, where the sum is taken over odd and even bonds, respectively. The decomposition leads to a two-dimensional classical model with a checkerboard structure (Fig. 1 (a)) and plaquette interactions τ given by

$$\tau_{l_2 r_2}^{l_1 r_1} = \begin{array}{c} r_1 \quad r_2 \\ \text{shaded square} \\ l_1 \quad l_2 \end{array} = \langle l_1 l_2 | e^{-\beta h_{i,i+1}} | r_1 r_2 \rangle. \quad (10)$$

The quantum direction L is thereby supplemented by a virtual Trotter dimension M . The plaquettes are column-wise combined to the quantum transfer matrix (QTM) T_M , cf. Fig. 1(a). Alternatively, the decomposition of the partition can be constructed³² as shown in Fig. 1(b), which is fully translational invariant in quantum direction, in contrast to (a). The advantage of (b) is discussed later, we first focus on variant (a).

One finds that the thermodynamics in the thermodynamic limit $L \rightarrow \infty$ is determined by the leading eigenvalues Λ_α and eigenvectors $|\Lambda_\alpha^{L/R}\rangle$ ($\alpha = 0, 1, \dots$) of T_M . Note, that left and right eigenvectors have to be distinguished because T_M is in general *not* symmetric. The free energy explicitly reads

$$f = -\frac{T}{2} \ln \Lambda_0 \quad (11)$$

where the leading eigenvalue Λ_0 is real and unique due to Frobenius' theorem. Thus, we always observe a gap in T_M , which only may close and lead to a phase transition for $M \rightarrow \infty$ ($T \rightarrow 0$). The expectation value of any local operator O_j is given by

$$\langle O_j \rangle = \frac{\langle \Lambda_0^L | T_M(O_j) | \Lambda_0^R \rangle}{\Lambda_0} \quad (12)$$

where in $T_M(O_j)$ one plaquette of the QTM T_M has been modified by the operator O_j .

In the TMRG algorithm, the matrices T_M and $T_M(O_j)$ are sequentially enlarged using a DMRG-like algorithm. An asymmetric density matrix $\rho = \text{tr}' |\Lambda_0^R\rangle \langle \Lambda_0^L|$ is used to target the leading eigenvector. We do not discuss the details, since the TMRG we use basically follows Ref. 27, 28. As spin and particle number are conserved by \mathcal{H} , T_M has a block structure that drastically reduces the computational effort. Alternatively, we use the number of particles with spin up and down $N_\sigma = \sum_i n_{i\sigma}$ to build the QTM blocks. To be more precise, N_σ are conserved for a row-transfer matrix. Contrary, $\Delta N_\sigma = \sum_i (-1)^i n_{i\sigma}$ are the corresponding good quantum numbers for the (column) quantum transfer matrix T_M .²⁸ Hence, we label the QTM block by the tuple $(\Delta N_\uparrow, \Delta N_\downarrow)$. The leading eigenvalue Λ_0 is located in the $(0, 0)$ block. This follows directly from the high temperature limit $T \rightarrow \infty$, where $e^{-\beta h_{i,i+1}}$ is unity and therefore

$$\tau_{l_2 r_2}^{l_1 r_1} = \delta_{l_2 r_2} \delta_{l_1 r_1}. \quad (13)$$

Thus, only matrix elements of the $(0, 0)$ block of T_M are non-vanishing. Consequently Λ_0 is also found in the $(0, 0)$ block. This property persists for finite temperatures $T > 0$, because no level crossing is expected, which would imply a phase transition.

B. Correlation lengths

One focus of the present work are correlation functions, such as spin, density and superconducting pair correlations. The general form of a two-point correlation function $\langle O_0^\dagger O_j \rangle$ for a local operator O_j at finite temperatures reads

$$\langle O_0^\dagger O_j \rangle - \langle O_0^\dagger \rangle \langle O_j \rangle = \sum_\alpha M_\alpha e^{-j/\xi_\alpha} e^{ik_\alpha j}. \quad (14)$$

All correlations decay exponentially because no phase transition can occur for $T > 0$. The correlation lengths (CL) are directly accessible by the leading eigenvalues

$$\xi_\alpha^{-1} = \frac{1}{2} \ln \frac{\Lambda_0}{|\Lambda_\alpha|}. \quad (15)$$

The wavevectors k_α are given by the complex argument

$$k_\alpha = \frac{1}{2} \arg \left(\frac{\Lambda_0}{\Lambda_\alpha} \right) + n\pi \quad (n = 0, 1). \quad (16)$$

As the classical lattice in Fig. 1(a) is translational invariant in quantum direction, but with a doubled unit cell, k_α is only determined modulo π . This problem can be solved by using the QTM presented in Fig. 1(b), cf. ref. 32.

The crucial question which eigenvalue Λ_α refers to which correlation function is controlled by the coefficients M_α , that are given by²⁸

$$M_\alpha = \frac{\langle \Lambda_0^L | T_M(O_j^\dagger) | \Lambda_\alpha^R \rangle \langle \Lambda_\alpha^L | T_M(O_j) | \Lambda_0^R \rangle}{\Lambda_0 \Lambda_\alpha}. \quad (17)$$

Eq. (17) represents a selection rule to assign Λ_α to the correct *type* of correlation length. A first criterion are the quantum numbers $(\Delta N_\uparrow, \Delta N_\downarrow)$ of $|\Lambda_\alpha^{L/R}\rangle$: M_α is non-vanishing only, if $\langle \Lambda_\alpha^L |$ and $T_M(O_j) | \Lambda_0^R \rangle$ have the same quantum numbers. To be more concrete, we discuss now the relevant correlation functions.

Longitudinal spin ($O_j = n_{j\uparrow} - n_{j\downarrow}$) and charge ($O_j = n_{j\uparrow} + n_{j\downarrow}$) correlations are determined by eigenvalues Λ_α of the $(0, 0)$ block of T_M , since O_j is diagonal and $T_M(O_j)$ does not change the quantum numbers. They have to be distinguished by calculating M_α explicitly.

The situation changes for the superconducting singlet and triplet pair correlations, where O_j in eq. (14) is given by

$$P_j^s = \frac{1}{\sqrt{2}} (c_{j\uparrow} c_{j+1\downarrow} - c_{j\downarrow} c_{j+1\uparrow}), \quad (18)$$

$$P_j^{t1} = \frac{1}{\sqrt{2}} (c_{j\uparrow} c_{j+1\downarrow} + c_{j\downarrow} c_{j+1\uparrow}), \quad (19)$$

$$P_j^{t2} = c_{j\uparrow} c_{j+1\uparrow}, \quad P_j^{t3} = c_{j\downarrow} c_{j+1\downarrow}. \quad (20)$$

The pair correlation operators change the quantum numbers. Therefore, eigenvalues Λ_α of the $(\pm 1, \pm 1)$ block contribute to the correlation lengths of P_j^s and P_j^{t1} , whereas those of the $(\pm 2, 0)$ and $(0, \pm 2)$ block belong to P_j^{t2} and P_j^{t3} , respectively. Without magnetic field, the triplet correlation functions P_j^{ti} are equal. Thus one can unambiguously distinguish singlet and triplet pair correlation lengths by computing the eigenvalues Λ_α of the $(1, 1)$ and $(2, 0)$ block only.

Note, that the present work uses both types of QTMs of Fig. 1. Even if the second variant improves the calculation of k_α , the checkerboard style QTM (Fig. 1(a)) is more precise, especially for the correlation lengths. The reasons for that are technical ones within the TMRG algorithm.

C. Jordan-Wigner Transformation

A sophisticated point in the TMRG algorithm are the fermion statistics which have *not* been considered in the Suzuki-Trotter mapping in eq. (9). Hence we use a Jordan-Wigner transformation (JWT)⁴¹ to map the fermion system onto a spin model. We define two unitary operators

$$K_{j\uparrow} = \exp \left(i\pi \sum_{i=1}^{j-1} \sum_{\sigma=\uparrow,\downarrow} S_{i\sigma}^+ S_{i\sigma}^- \right), \quad (21)$$

$$K_{j\downarrow} = \exp \left(i\pi \sum_{i=1}^j \sum_{\sigma=\uparrow,\downarrow} S_{i\sigma}^+ S_{i\sigma}^- \right) \quad (22)$$

where $S_{i\sigma}^-$ ($S_{i\sigma}^+$) are spin-1/2 lowering (raising) matrices of two "spin types" $\sigma = \uparrow, \downarrow$ at site i . These are related to the fermion operators by

$$c_{j\sigma} = K_{j\sigma} S_{j\sigma}^- \quad \text{and} \quad c_{j\sigma}^\dagger = S_{j\sigma}^+ K_{j\sigma}. \quad (23)$$

These operators fulfill the Fermi statistics. Inserting the JWT into the Hamiltonian (1), the hopping terms $c_i^\dagger c_j$ modify, whereas the diagonal charge operators $n_{i\sigma}$ transform canonically:

$$\begin{aligned} c_{i+1\uparrow}^\dagger c_{i\uparrow} &\rightarrow (-1)^{n_{i\downarrow}} S_{i+1\uparrow}^+ S_{i\uparrow}^- \\ c_{i+1\downarrow}^\dagger c_{i\downarrow} &\rightarrow (-1)^{n_{i+1\uparrow}} S_{i+1\downarrow}^+ S_{i\downarrow}^- \\ n_{i\sigma} &\rightarrow S_{i\sigma}^+ S_{i\sigma}^- \end{aligned} \quad (24)$$

Note that periodic boundary conditions may transform to twisted ones, but this is irrelevant for our studies where the thermodynamic limit is performed exactly. We point out that without the JWT the TMRG algorithm computes wrong results in particular for the singlet correlation lengths of the $(\pm 1, \pm 1)$ block, although many other quantities are not affected.

IV. RESULTS

We present numerical TMRG results for the parameter region $0 \leq X/t \leq 1$, which is representative for all X/t , cf. Sec. II. In all computations we have set $t = 1$ and temperatures are measured in units of t . As we use a grand canonical description, the chemical potential μ controls the density n of particles. Note, that the density is therefore temperature dependent, $n = n(T, \mu)$. If not stated differently, we use $\epsilon = 0.05$ and retain $N = 70 - 100$ states in the TMRG algorithm. This is already sufficient for highly accurate results. We typically compute $M \approx 1000$ TMRG iterations, which correspond to a minimal reachable temperature of $T = 0.02$.

A. Thermodynamics

In this section we analyze various thermodynamic quantities: the grand canonical potential ϕ , local ex-

pectation values (e.g. local density n), charge and spin susceptibilities χ_c and χ_s and the specific heat c_μ .

The grand canonical potential $\phi(T, \mu)$ is directly accessible through the largest eigenvalue of the QTM, cf. Sec. III. The charge susceptibility

$$\chi_c(T, \mu) = \left. \frac{\partial n}{\partial \mu} \right|_T \quad (25)$$

is obtained by computing the density $n = \langle n_{i\uparrow} + n_{i\downarrow} \rangle$ of electrons for two different chemical potentials $\mu - \Delta\mu$ and $\mu + \Delta\mu$. Then, we use numerical derivatives

$$\chi_c(T, \mu) \approx \frac{n(T, \mu + \Delta\mu) - n(T, \mu - \Delta\mu)}{2\Delta\mu} \quad (26)$$

to approximate χ_c , where typically $\Delta\mu \sim 10^{-2}$ is chosen. Similarly, the spin susceptibility

$$\chi_s|_{h=0} = \left. \frac{\partial m}{\partial h} \right|_{\mu, T; h=0} \quad (27)$$

is obtained by the numerical derivative of the magnetisation $m = \langle n_{i\uparrow} - n_{i\downarrow} \rangle$, varying the magnetic field h .

The natural form of the specific heat in a grand canonical formulation is given by

$$c_\mu = T \left. \frac{\partial s}{\partial T} \right|_\mu = T \left. \frac{\partial^2 \phi}{\partial T^2} \right|_\mu, \quad (28)$$

where s denotes the entropy per site. But usually one finds data for the specific heat at constant density n , which is related to c_μ by the thermodynamic relation

$$c_n = T \left. \frac{\partial s}{\partial T} \right|_n = c_\mu - T \left. \frac{\partial n}{\partial T} \right|_\mu \left. \frac{\partial \mu}{\partial n} \right|_T. \quad (29)$$

We only determine c_μ by calculate numerically the second derivative of the grand canonical potential ϕ .

1. Exactly Solvable Case $X = 1$

First, we show data for the exactly solvable case $X = 1$, basically to check the precision of the TMRG algorithm. In Fig. 2 the grand canonical potential ϕ is plotted for the chemical potentials $\mu = -0.5, 0, 0.5$. The temperature dependence of the density $n(T, \mu)$ is plotted in the upper inset. The particle-hole symmetry of the model is confirmed by the symmetry of $n(T, \pm 0.5)$ as well as by the potentials $\phi(T, \pm 0.5)$, which are only shifted by $\Delta\mu = 1$. Our data are compared to exact results, calculated by eq. (7), cf. the lower inset of Fig. 2. The absolute error is less than 10^{-4} for temperatures $T > 0.1$ and less than 10^{-3} for $0.02 < T < 0.1$. Not explicitly shown here, the errors of the density n as well as other expectation values (e.g. the magnetisation) are approximately of the same order.

The origin of a numerical error of at least 10^{-3} can be understood by the approximation done in the Suzuki-Trotter decomposition in eq. (9). The choice of ϵ (in our

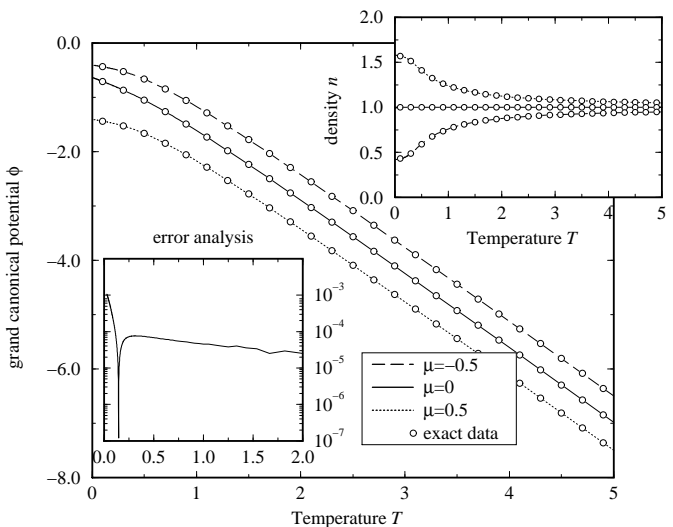


FIG. 2: (left) Grand canonical potential ϕ as function of temperature for $X = 1$ and chemical potentials $\mu = -0.5, 0, 0.5$. The absolute deviation from the exact value in dependence of the temperature is plotted in the left inset for $\mu = 0$. The corresponding TMRG data for the density $n = n(T, \mu)$ is depicted in the right inset. For comparison exact data using eq. (7) are shown by circles (\circ).

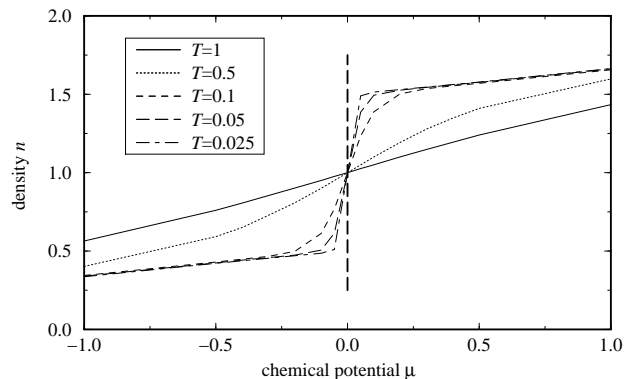


FIG. 3: Density $n(\mu, T)$ as a function of temperature and chemical potential for $X = 1$. For $T \rightarrow 0$ a discontinuity at $\mu = 0$ is found, where the density jumps from $n = 0.5$ to $n = 1.5$.

case $\epsilon = 0.05$) causes an error of the order $\mathcal{O}(\epsilon^2)$ in the partition function (9).

It is interesting to investigate also the density $n(T, \mu)$ as a function of μ and T (Fig. 3). For $T \rightarrow 0$ one observes the formation of a plateau for $\mu = 0$. This can be explained by the ground states of the η -pair phase, which occurs for $0.5 < n < 1.5$. Here, all ground states with different numbers of pairs $N_{\uparrow\downarrow}$ are degenerate. Thus the chemical potential does not change by adding a particle, because a new bound pair is build without changing the energy. Thus, the thermodynamics of the η -pair phase can be only realized for $\mu = 0$. Any $\mu \neq 0$ induces $n < 0.5$ or $n > 1.5$ and falls into the $U = \infty$ phase, cf. Sec. II.

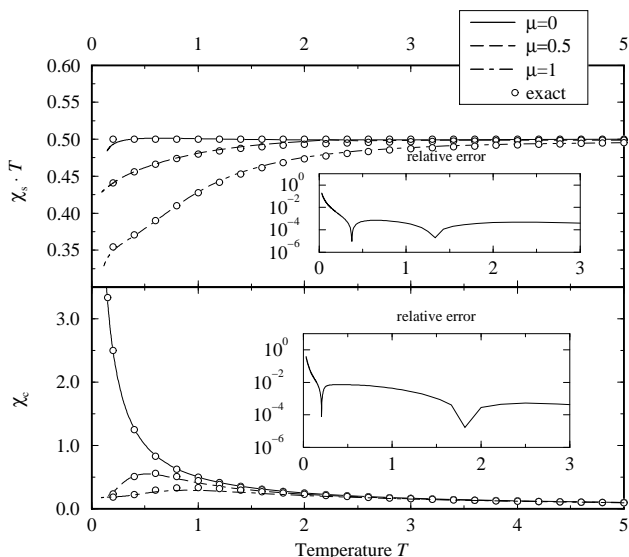


FIG. 4: Spin and charge susceptibility as a function of temperature for $X = 1$ and $\mu = 0, 0.5, 1.0$. The upper diagram plots $\chi_s \cdot T$ over T in order to demonstrate that χ_s diverges like $\chi_s \sim 1/T$. The insets depict the relative deviation from exact results for $\mu = 0$.

Fig. 4 depicts the spin and charge susceptibilities for $X = 1$ and $\mu = 0, 0.5, 1.0$. The comparison with exact data results in a relative error less than 10^{-2} for temperatures $T \gtrsim 0.1$. Not surprisingly, it is larger than that for ϕ , because numerical errors are propagating through the numerical derivatives.

From conformal field theory (CFT) the low temperature limit $T \rightarrow 0$ of χ_s and χ_c are respectively given by

$$\chi_s(T \rightarrow 0) = \frac{2}{\pi v_s} \quad \text{and} \quad \chi_c(T \rightarrow 0) = \frac{2K_c}{\pi v_c}, \quad (30)$$

where v_s and v_c denote the spin and charge velocities and K_c the LL parameter. This can be used to interpret the results of Fig. 4. The ground states of $X = 1$ for $n < 0.5$ (and after particle-hole transformation for $n > 1.5$) corresponds to the $U = \infty$ Hubbard model, cf. Sec. II. For the $U = \infty$ Hubbard model it is known, that

$$v_s = 0 \quad \text{and} \quad v_c = 2t|\sin(\pi n)|. \quad (31)$$

The spin excitations exhibit no dispersion due to complete degeneracy²¹. In Fig. 4 we have plotted $\chi_s \cdot T$ to demonstrate, that the spin susceptibility χ_s is diverging for all μ and fillings n in the limit $T \rightarrow 0$ since $\lim_{T \rightarrow 0} T\chi_s$ is finite. The charge susceptibility χ_c is divergent for $\mu = 0$.

2. Non-Integrable Case $0 < X < 1$

We now consider the non-integrable case $0 < X < 1$. From analytical^{7,8} and numerical^{13,14,15} approaches it is

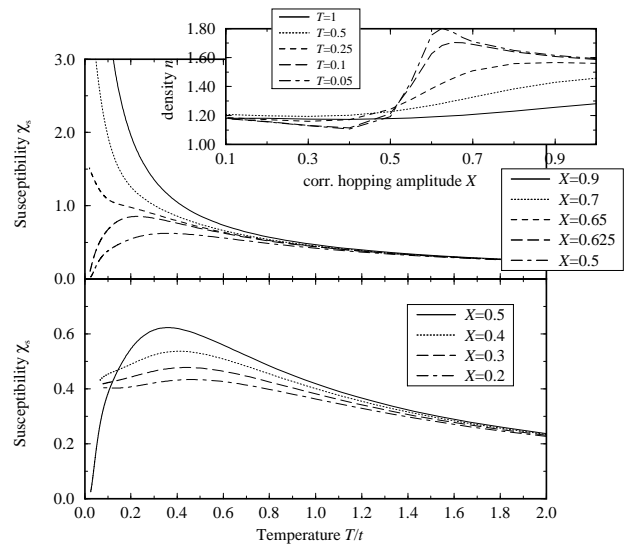


FIG. 5: Spin susceptibility as a function of temperature for various amplitudes $X/t = 0.9 \dots 0.1$ and fixed chemical potential $\mu = 0.6$. The upper figure shows χ_s for $X = 0.9 \dots 0.5$ the lower one for $X = 0.1 \dots 0.5$, respectively. The inset depicts the density $n(X, \mu = 0.6, T)$ for various parameters X .

known, that a crossover from a TLL phase to a superconducting LEL is observed. For $X \ll 1$ this is evident, because the bond-charge model is an effective Hubbard model (cf. Sec. II), where the crossover is expected to appear at $U_{\text{eff}} = 0$, corresponding to half-filling $n = 1$ (see (4)).

In our thermodynamic study we can identify the existence of a spin gap if the susceptibility χ_s vanishes for $T \rightarrow 0$. In Fig. 5 χ_s is depicted for fixed chemical potential $\mu = 0.6$ and various hopping amplitudes $0 < X < 1$. For $X > 0.65$ we can clearly verify TLL behaviour, because the susceptibility does not vanish for $T \rightarrow 0$. At $X \approx 0.65$ we observe a crossover to a LEL phase with $\chi_s(T \rightarrow 0) = 0$. Decreasing X further, the gap seems to close again for $X \lesssim 0.3$.

Additional the inset of Fig. 5 shows the density $n(T, \mu = 0.6)$ for the respective parameters X . Note, that $\mu = 0.6$ induces a regime of more than half filling $n > 1$ for each X . Therefore the spin gap should persist especially for $X \ll 1$, which we can not show by our TMRG results. But from the attractive Hubbard model it is known, that the spin gap is exponentially small for $U \ll 1$. Since from (4) we have $U_{\text{eff}} \ll 1$ for $X \ll 1$, the gap in the bond-charge model becomes extremely small, especially at half filling. The decay of χ_s at $X \ll 1$ is therefore expected at such low temperatures that are not accessible by TMRG. To verify that all $X \leq 0.5$ exhibit a spin gap we increased the filling in Fig. 6. Here, the effective Coulomb potential U_{eff} is larger and the spin gap appears in our data.

In order to give a more detailed overview of the thermodynamics of the bond-charge model for $0 < X < 1$, we focus on three particular points $X = 0.1, 0.5, 0.9$.

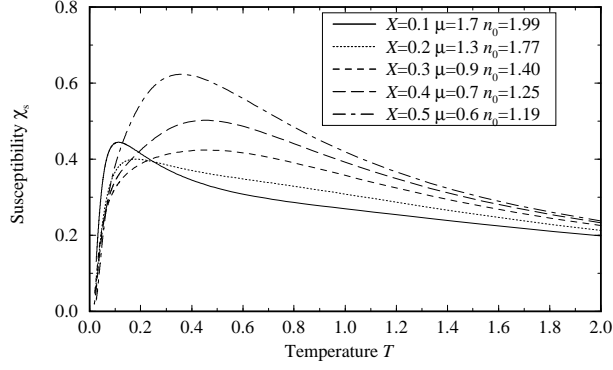


FIG. 6: Spin susceptibility χ_s as a function of temperature for the parameter region $X = 0.5 \dots 0.1$ and sufficiently large fillings. The respective densities $n_0 = n(\mu, T \rightarrow 0)$ are given in the legend.

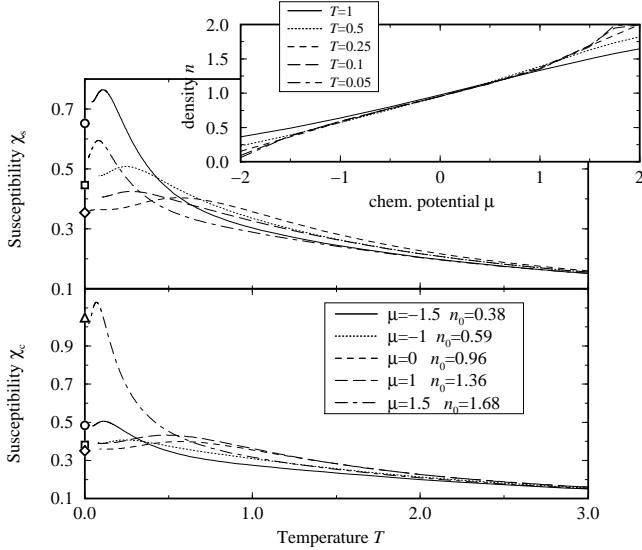


FIG. 7: Spin and charge susceptibilities χ_s and χ_c as a function of temperature for $X/t = 0.1$ and various chemical potentials μ . The inset plots the density $n(\mu, T)$. The corresponding $T = 0$ values for the Hubbard model with effective U_{eff} and t_{eff} are shown by symbols, (\circ) : $\mu = -1.5$, (\square) : $\mu = -1$, (\diamond) : $\mu = 0$ and (\triangle) : $\mu = 1.5$.

Fig. 7 plots the charge and spin susceptibility at $X = 0.1$ for various chemical potentials μ . Additionally, in the inset, the density $n(\mu, T)$ is depicted. As X is small compared to the bandwidth t , the model (1) should coincide with the effective Hubbard model. We check the asymptotics of the susceptibilities χ_s and χ_c for $T \rightarrow 0$ using eq. (30). These can be calculated exactly for the integrable Hubbard model^{42,43}. For a weak (repulsive)

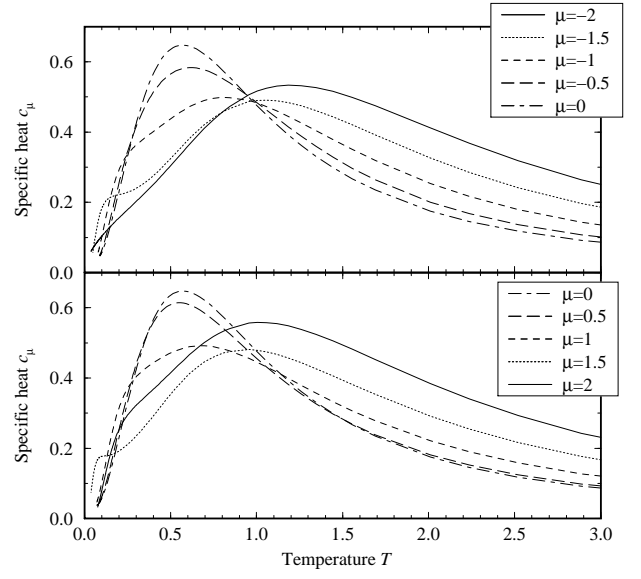


FIG. 8: Specific heat c_μ as a function of temperature for $X = 0.1$ and chemical potentials $\mu \leq 0$ (upper figure) and $\mu \geq 0$ (lower figure).

Coulomb potential U , one finds

$$v_{c/s} = v_F \left(1 \pm \frac{U}{4\pi t \sin k_F} \right) = v_F \pm \frac{U}{2\pi}, \quad (32)$$

$$K_c = 1 - \frac{U}{4\pi t \sin(k_F)} \quad (33)$$

with $v_F = 2t \sin(k_F)$ and $k_F = \frac{n\pi}{2}$. Using eqs. (32), (33) and (30) we have calculated χ_s and χ_c for $T \rightarrow 0$ (see Fig. 7). The density $n_0 = n(\mu, T \rightarrow 0)$ which was used to determine k_F , U_{eff} and t_{eff} is denoted in the legend of Fig. 7. We observe perfect agreement with our data, which again supports the correspondence of (effective) Hubbard and bond-charge model.

Even more evidence of Hubbard like thermodynamics is given by the shape of the specific heat c_μ . As shown for c_μ in Fig. 8, two characteristic features can be observed for large and small fillings, a shoulder at low temperatures and a peak at a slightly larger temperature. As in the repulsive Hubbard model these features can be related to spin and charge excitations, respectively. They merge close to half filling where we have effectively a free fermion system for $X \ll 1$. Moreover the regime less than half filling $n < 1$ closely corresponds to $n > 1$. Again, this can be explained by the exponentially small gap, which does not affect the physics at those temperature scales we can observe by TMRG.

The effect of the spin gap manifests itself at larger interactions X . Fig. 9 depicts charge and spin susceptibilities for $X = 0.5$. In contrast to $X = 0.1$, the spin susceptibility χ_s clearly affirms a gap for $n > 1$ since $\chi_s(T \rightarrow 0) \rightarrow 0$. Therefore the phase transition occurs at half filling, which is predicted by the bosonisation results⁷. A significantly larger spin gap than at $X = 0.1$

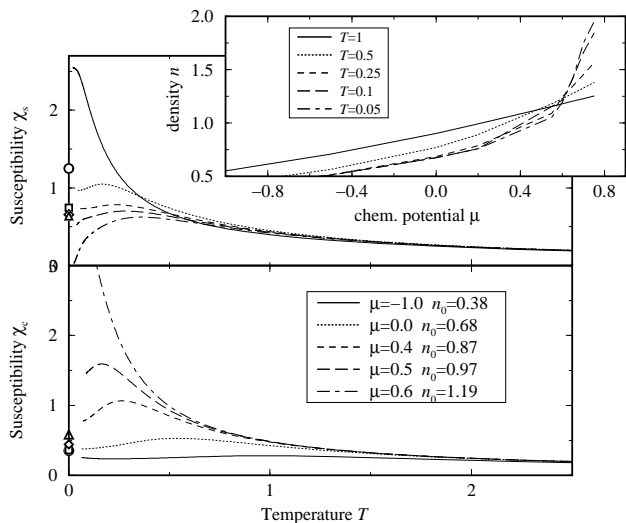


FIG. 9: Spin and charge susceptibilities χ_s and χ_c as a function of temperature are depicted for $X = 0.5$ and various chemical potentials μ . The inset plots the density $n(\mu, T)$. The corresponding $T = 0$ values for χ_s and χ_c calculated from the Hubbard model with effective U_{eff} and t_{eff} are shown by symbols, (\circ) : $\mu = -1$, (\square) : $\mu = 0$, (\diamond) : $\mu = 0.4$ and (\triangle) : $\mu = 0.5$.

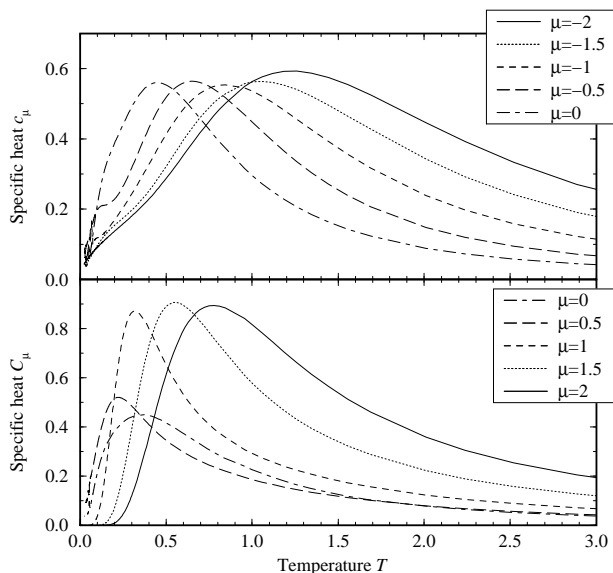


FIG. 10: Specific heat c_μ as a function of temperature for $X = 0.5$ and various chemical potentials $\mu < 0$ (upper figure) and $\mu > 0$ (lower figure).

is also verified by the specific heat shown in Fig. 10. The linear behaviour of c_μ for $\mu \gtrsim 1$ occurs only at very low temperatures and can not be observed on the temperature scale shown. Here the exponential corrections coming from the finite spin gap dominate.

Even though the numerical data for the thermodynamics suggest Hubbard like behaviour on a qualitative level, a more detailed quantitative comparison fails for

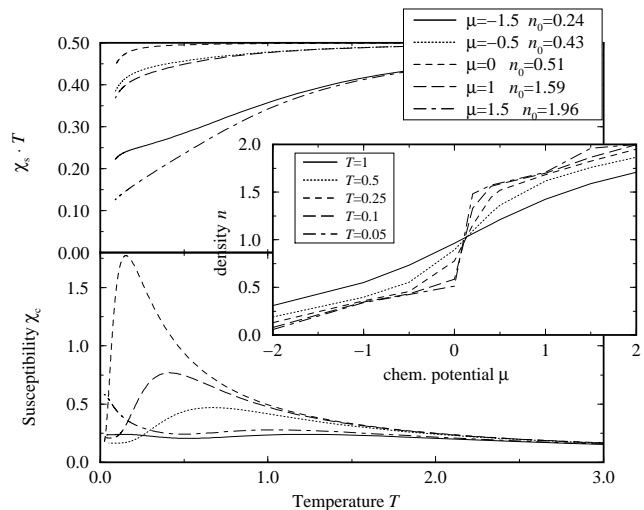


FIG. 11: Spin and charge susceptibilities χ_s and χ_c are depicted for $X = 0.9$ and various chemical potentials μ . The inset shows the density $n(\mu, T)$.

$X = 0.5$. Since U_{eff} is not small here, we used the Bethe Ansatz (instead of eq. (32) and (33)) to calculate the $T \rightarrow 0$ values of χ_s and χ_c for the (effective) Hubbard model, which are also depicted in Fig. 9. Obviously, these do not fit to our TMRG data.

For large $X \approx 1$ the spin gapped phase disappears, which also contradicts the results of bosonisation. As an example we show TMRG data for $X = 0.9$. The susceptibilities and the density, which are shown in Fig. 11, qualitatively coincide with the $X = 1$ case. At $\mu \approx 0$ we observe a jump in the density, indicating a phase comparable to the η -pair phase. The spin susceptibility $\chi_s(T \rightarrow 0)$ is diverging for all fillings n , which yields $v_s \rightarrow 0$. Fig. 12 additionally plots the specific heat c_μ for various chemical potentials μ . In fact the model is observed to be nearly particle-hole symmetric ($\mu \rightarrow -\mu$). Note, that for $\mu = 0$ the specific heat exhibits an additional low energy peak. Spin excitations can not contribute to that peak due to complete degeneracy. For $X = 1$ such peak has also been observed in ref. 21. It is associated with the melting of pairs. Remarkably, the physics at $X = 0.9$ is very similar to the highly symmetric $X = 1$ case. Thus, $X = 1$ is not a singular point, but the characteristics persist for a certain neighbourhood around $X = 1$.

3. Universal Crossing Points

In the thermodynamic data shown above we find various phenomena of (nearly) universal crossing points. As a first example, the specific heat in Fig. 8 exhibits even two crossing points. But also in the density in Fig. 7 or Fig. 9 a crossing point is apparent at $n \approx 1$.

In the case of the Hubbard model, it is well known⁴⁴

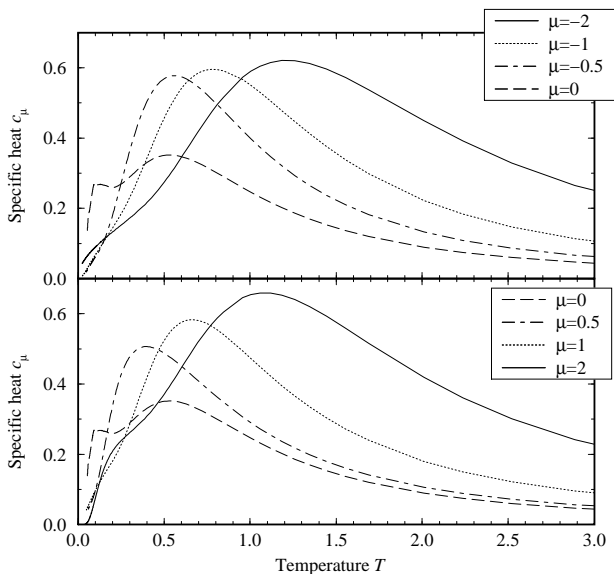


FIG. 12: Specific heat c_μ as a function of temperature for $X = 0.9$ and various chemical potentials $\mu \leq 0$ (upper figure) and $\mu \geq 0$ (lower figure).

that such crossing points appear. In refs. 45,46 general thermodynamic arguments for the existence of a sharp crossing point in the specific heat are given.

Sharp universal crossing points (μ_c, n_c) in the density $n = n(T, \mu)$ can be generally explained in a similar way. The integral

$$\int_{-\infty}^{\infty} \frac{\partial n}{\partial T} \Big|_{\mu} d\mu = \int_{-\infty}^{\infty} \frac{\partial s}{\partial \mu} \Big|_T d\mu = s(\infty, T) - s(-\infty, T) = 0 \quad (34)$$

vanishes: for $\mu \rightarrow \pm\infty$ the band is either completely empty or filled, thus $s \rightarrow 0$. Then $\frac{\partial n}{\partial T} \Big|_{\mu}$ has to change its sign. Due to continuity arguments we conclude the existence of μ_c , such that

$$\frac{\partial n}{\partial T} \Big|_{\mu_c} = 0 \implies n(T, \mu_c) = \text{const.} \quad (35)$$

In the case of the bond-charge model at weak coupling $X \ll 1$, the crossing point of the density appears at half filling $n_c = 1$, where the model effectively behaves as free fermions ($U_{\text{eff}} = 0$).

B. Correlation Lengths

A great advantage of the TMRG algorithm is that not only quantities related to the free energy (11) are accessible, but also, through the next-leading eigenvalues of the transfer matrix, thermal correlation lengths (15). As explained in Sec. III B, the corresponding correlation functions are identified by their quantum numbers $(\Delta N_{\uparrow}, \Delta N_{\downarrow})$. It is even possible to distinguish

the contributions of different wavevectors $k_\alpha = \alpha k_F$ ($\alpha = 0, 2, 4, \dots$). This will be done in the following to determine the dominant correlations in the different parameter regimes. First we discuss the low-temperature behaviour, which can be compared to predictions of conformal field theory.

1. Low-temperature behaviour

The correlation functions of a TLL at temperature $T = 0$ show universal behaviour. According to conformal field theory (CFT), density-density (d-d), spin-spin (s-s), singlet pair (sp) and triplet pair (tp) correlation functions read^{7,47}

$$\langle n_r n_0 \rangle \sim A_0 r^{-2} + A_1 r^{-(1+K_c)} \cos(2k_F r) + A_2 r^{-4K_c} \cos(4k_F r), \quad (36)$$

$$\langle S_r^z S_0^z \rangle \sim B_0 r^{-2} + B_1 r^{-(1+K_c)} \cos(2k_F r), \quad (37)$$

$$\langle P_r^{s\dagger} P_0^s \rangle \sim C_0 r^{-(1+\frac{1}{K_c})} + C_1 r^{-(K_c+\frac{1}{K_c})} \cos(2k_F r), \quad (38)$$

$$\langle P_r^{t\dagger} P_0^t \rangle \sim D_0 r^{-(1+\frac{1}{K_c})} + D_1 r^{-(K_c+\frac{1}{K_c}+2)} \cos(2k_F r) \quad (39)$$

(up to logarithmic corrections). Thus, all critical exponents are controlled by a dimensionless parameter K_c .

In contrast, in a LEL the spin excitations are gapped. Thus s-s and tp correlations decay exponentially and do not show universal behaviour. According to CFT, the asymptotic behaviour of the d-d and sp correlations is given by^{7,47}

$$\langle n_r n_0 \rangle \sim A_0 r^{-2} + A_1 r^{-K_c} \cos(2k_F r) + A_2 r^{-4K_c} \cos(4k_F r), \quad (40)$$

$$\langle P_r^{s\dagger} P_0^s \rangle \sim C_0 r^{-\frac{1}{K_c}} + C_1 r^{-(K_c+\frac{1}{K_c})} \cos(2k_F r). \quad (41)$$

In the present work we are discussing correlation functions at *finite* temperatures $T > 0$. Here, the model is always non-critical and all correlation functions decay exponentially. The asymptotics are described in terms of thermal correlation lengths (CL), cf. eq. (14), which are temperature dependent.

The asymptotic behaviour of the CL for small temperatures $T \rightarrow 0$ can still be obtained by CFT³³. For a TLL all CLs diverge

$$\xi(T \rightarrow 0) = \frac{1}{2\pi T \left(\frac{x_c}{v_c} + \frac{x_s}{v_s} \right)} =: \frac{\gamma}{T}. \quad (42)$$

The scaling dimensions x_s and x_c can be calculated explicitly. One finds, that the non-oscillating d-d (s-s) CL is given by

$$\gamma_{\text{dd}}^{(0)} = \frac{v_c}{2\pi}, \quad \gamma_{\text{ss}}^{(0)} = \frac{v_s}{2\pi}. \quad (43)$$

The $2k_F$ parts of both read

$$\gamma_{\text{dd/ss}}^{(2k_F)} = \frac{v_c}{\pi \left(\frac{v_c}{v_s} + K_c \right)} \quad (44)$$

whereas the $4k_F$ part of the d-d CL yields

$$\gamma_{\text{dd}}^{(4k_F)} = \frac{v_c}{4\pi K_c}. \quad (45)$$

The non-oscillating parts of sp and tp CL are given by

$$\gamma_{\text{sp/cp}}^{(0)} = \frac{v_c}{\pi \left(\frac{1}{K_c} + \frac{v_c}{v_s} \right)}, \quad (46)$$

the $2k_F$ part of the sp CL by

$$\gamma_{\text{sp}}^{(2k_F)} = \frac{v_c}{\pi \left(\frac{1}{K_c} + K_c \right)} \quad (47)$$

and the $2k_F$ part of the tp CL by

$$\gamma_{\text{tp}}^{(2k_F)} = \frac{v_c}{\pi \left(\frac{1}{K_c} + K_c + 2\frac{v_c}{v_s} \right)}. \quad (48)$$

In the LEL the tp and s-s CLs do not diverge for $T \rightarrow 0$ due to the spin gap. But the asymptotic behaviour of the d-d and sp CLs is still predictable by CFT and corresponds to eq. (43)-(47) in the limit $v_s \rightarrow \infty$. Thus, we have

$$\gamma_{\text{dd}}^{(0)} = \frac{v_c}{2\pi}, \quad \gamma_{\text{dd}}^{(2k_F)} = \frac{v_c}{\pi K_c} \quad \text{and} \quad \gamma_{\text{dd}}^{(4k_F)} = \frac{v_c}{4\pi K_c} \quad (49)$$

for the non-oscillating, $2k_F$ and $4k_F$ d-d CLs and

$$\gamma_{\text{sp}}^{(0)} = \frac{v_c K_c}{\pi} \quad \text{and} \quad \gamma_{\text{sp}}^{(2k_F)} = \frac{v_c}{\pi \left(\frac{1}{K_c} + K_c \right)} \quad (50)$$

for the non-oscillating and $2k_F$ sp CL, respectively. Note, that the low temperature asymptotics of the correlation lengths depend not only on the universal exponent K_c , but additionally on the charge and spin velocities v_c and v_s .

2. Comparison of correlation lengths

It was shown in Sec. III that the TMRG algorithm provides a very effective facility to compute thermal correlation lengths numerically. First, we check the precision of our TMRG data. For that purpose we choose $X = 0$, which describes a system of free fermions with spin. Here, all correlation lengths can be computed exactly. Due to Wick's theorem, spin, charge and pair CLs are identical given by³³

$$\xi^{-1} = 2 \operatorname{arsinh}(\pi T/2). \quad (51)$$

Fig. 13 compares the CLs computed by the TMRG program to exact data. Down to a temperature $T \approx 0.2$

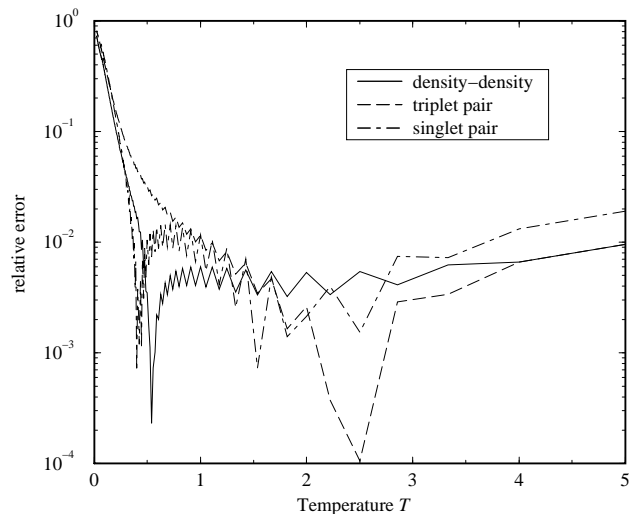


FIG. 13: Precision check of various correlation lengths computed by the TMRG algorithm for free fermions. The relative error is plotted as a function of temperature T , showing that the CLs keep reliable for $T > 0.2$.

the relative error is shown to be less than 10%. As already mentioned in Sec. III it is important to perform a JWT before applying the TMRG to the bond-charge model. Otherwise, particularly the singlet pair correlations are *not* correctly reproduced by the algorithm.

We now discuss in detail s-s, d-d, sp and tp correlations in the bond-charge model. We focus on the parameter point $X = 0.5$, where the spin gap is comparatively large for $n \gtrsim 1$. For $T = 0$, the system is then a LEL with dominating superconducting sp correlations due to $K_c > 1$.¹³ From eqs. (49) and (50) it is expected, that sp correlations should dominate even for finite low temperatures $T > 0$. At zero temperature, close to half-filling a transition to a TLL takes place which exists for all densities $n \lesssim 1$.

Fig. 14 shows the (leading) thermal CLs for three different chemical potentials ($\mu = -1, 0.4, 0.6$). The choice of μ covers the TLL ($\mu = -1$) and the LEL phase ($\mu = 0.6$) as well as a point close to the phase transition ($\mu = 0.4$). In these figures we have plotted $\xi \cdot T$ vs. T which allows to determine the low temperature asymptotics. As $\xi = \gamma/T$ for $T \rightarrow 0$ (cf. eq. (42)), the curves should become linear and intersect the ordinate at γ . According to CFT (see Sec. IV B 1), the factor γ depends on the spin and charge velocities and the critical exponent K_c .

For $\mu = -1$ ($n_0 \approx 0.38$) in Fig. 14 (a) the system is in the TLL regime. The non-oscillating d-d CL dominates for all temperatures. The leading s-s CL for $T \rightarrow 0$ shows incommensurate oscillations ($k = 2k_F$), whereas the $k = 0$ part is strongly suppressed and not shown in the figure. Additionally, the $k = 4k_F$ d-d correlation lengths dominate the $k = 2k_F$ d-d and all s-s CLs. This scenario can be easily understood by the fact, that the spin velocity is very small ($v_s \ll v_c$), which can be ver-

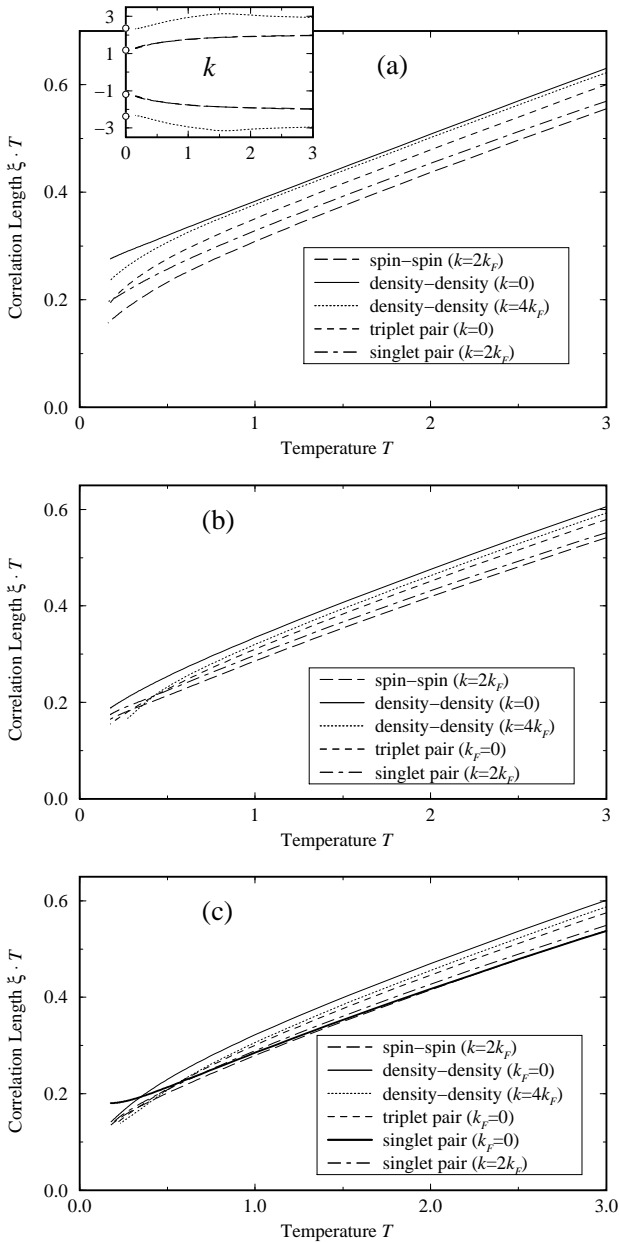


FIG. 14: Plot of the leading d-d, s-s, sp and tp correlation lengths ξ for $X = 0.5$ and (a) $\mu = -1$, (b) $\mu = 0.4$ and (c) $\mu = 0.6$. The corresponding densities $n_0 = n(T \rightarrow 0)$ read (a) $n_0 \approx 0.38$, (b) $n_0 \approx 0.88$ and (c) $n_0 = 1.19$. The diagrams show the respective correlation $\xi \cdot T$ as a function of T . As an example, the inset of (a) depicts the wavevectors k of the oscillating CLs. The circles (o) correspond to the $T \rightarrow 0$ limit of $k = 2k_F$ and $k = 4k_F$ with $k_F = n\pi/2$.

ified by Fig. 9. The ratio $v_c/v_s \gg 1$ enters eq. (44), thus these correlations are suppressed for low temperatures. For the same reason, the tp correlation length is crossed over by the leading incommensurable sp correlation length at low temperatures, cf. eq. (46). The inset of Fig. 14 (a) depicts the wavevectors k_F . We have also plotted the $T \rightarrow 0$ values of $2k_F$ and $4k_F$ with $k_F = \frac{\pi}{2}n$

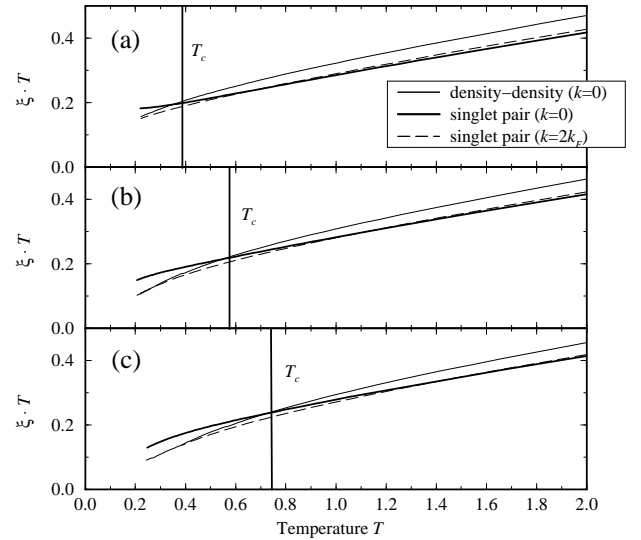


FIG. 15: Crossing phenomena of density-density ($k = 0$) and singlet pair ($k = 0, 2k_F$) correlation lengths for various chemical potentials (a) $\mu = 0.6$ (b) $\mu = 0.8$ and (c) $\mu = 1.0$. The diagrams plot the particular correlation length $\xi \cdot T$ as a function of temperature T . The corresponding densities $n_0 = n(T \rightarrow 0)$ are given by (a) $n_0 \approx 1.21$ (b) $n_0 \approx 1.92$ (c) $n_0 \approx 1.99$.

which agree perfectly with the TMRG data.

The case $\mu = 0.4$ ($n_0 \approx 0.88$) shown in Fig. 14 (b) also falls into the TLL regime, but is situated close to the phase transition to the LEL. The CLs generally get smaller, because the charge velocity v_c is decreased (Fig. 9). Note, that the crossing phenomena of CLs become very rich close to the transition.

A crossover of sp and d-d correlations at finite temperature $T_c \approx 0.5$ is observed in Fig. 14 (c) for $\mu = 0.6$ ($n_0 \approx 1.19$). And in contrast to the latter cases, the leading sp correlation length is shown to be commensurable. This agrees with the predictions of eq. (49) and (50), if $K_c > 1$ is assumed.

The crossing temperature T_c increases for higher fillings. This is demonstrated by Fig. 15, which shows only the leading d-d and sp correlation lengths for $\mu = 0.6, 0.8, 1.0$. Note, that the CLs in Fig. 14 (c) and Fig. 15 do not show asymptotic $\frac{1}{T}$ behaviour for the achievable temperature region $T > 0.2$.

V. CONCLUSIONS

In this paper we have studied in detail the thermodynamics of the bond-charge model by means of numerical TMRG calculations. We focused on the parameter region $0 \leq X/t \leq 1$, which is representative for the whole model due to particle-hole symmetry.

Our computations show data for the grand canonical potential, charge and spin susceptibilities, the specific heat, density and thermal correlations lengths. The de-

tailed study of small ($X/t = 0.1$), intermediate ($X = 0.5$) and large ($X = 0.9$) bond-charge coupling was performed to determine the underlying physics of the model.

In accordance with previous works, numerical studies of the spin and charge susceptibilities exhibit two $T = 0$ phases of the model. For less than half-filling we principally find Tomonaga-Luttinger liquid behaviour, where spin and charge excitations are gapless. For more than half-filling a Luther-Emery liquid phase with spin gap is found, if X is not too large.

We have shown that the thermodynamics for small $X \ll 1$ essentially coincide with that of the Hubbard with an effective Coulomb potential U_{eff} and hopping amplitude t_{eff} , as predicted by bosonisation. For intermediate coupling ($X = 0.5$) the correspondence holds qualitatively, but not quantitatively. For large $X \approx 1$, the spin gap disappears for all fillings, which even qualitatively contradicts the bosonisation results.

Additionally, numerical investigations of the specific heat and density exhibit interesting phenomena of nearly universal crossing points. These can be understood from quite general thermodynamic considerations.

Finally we focused on thermal correlation functions, which we characterized by thermal correlation lengths.

In the Luther-Emery liquid phase, we observed interesting crossing phenomena of superconducting singlet-pair and density-density correlations at finite temperatures $T_c > 0$. Even though true superconductivity is not possible in the one-dimensional bond-charge model, our studies support a *strong tendency* towards superconductivity. This indicates, that the bond-charge interaction may be relevant for superconducting phenomena in higher dimensions.

As we concentrated on the physics of correlated hopping only, additional interactions like on-site Coulomb repulsion U or pair hopping processes Y were not discussed in this paper. Work is in progress in these matters.

Acknowledgments

This work has been performed within the research program SFB 608 of the *Deutsche Forschungsgemeinschaft*. AK is supported by *Studienstiftung des Deutschen Volkes*. We would like to thank J. Sirker, A. Klümper and G. Japaridze for valuable discussions.

* kemper@thp.uni-koeln.de

† as@thp.uni-koeln.de

¹ J. E. Hirsch, Phys. Rev. B **65**, 184502 (2002).

² J. E. Hirsch (2003), preprint cond-mat/0301610.

³ J. E. Hirsch, Phys. Lett. A **134**, 452 (1989).

⁴ J. E. Hirsch, Physica C **158**, 326 (1989).

⁵ F. Marsiglio and J. E. Hirsch, Phys. Rev. B **41**, 6435 (1990).

⁶ R. Z. Bariev, A. Klümper, A. Schadschneider, and J. Zittartz, J. Phys. A: Math. Gen **26**, 1249 (1993).

⁷ G. I. Japaridze and E. Müller-Hartmann, Ann. Phys. (Lpz.) **3**, 163 (1994).

⁸ G. I. Japaridze and E. Müller-Hartmann, Ann. Phys. (Lpz.) **3**, 392 (1994).

⁹ F. Buzatu, Phys. Rev. B **49**, 10176 (1994).

¹⁰ B. Bulka, Phys. Rev. B **57**, 10303 (1998).

¹¹ A. Aligia, E. Gagliano, L. Arrachea, and K. Hallberg, Eur. Phys. J. B **5**, 371 (1998).

¹² G. I. Japaridze and A. P. Kampf, Phys. Rev. B **59**, 12882 (1999).

¹³ M. Quaiser, A. Schadschneider, and J. Zittartz, Europhys. Lett. **32**, 179 (1995).

¹⁴ M. Quaiser, Ph.D. thesis, University of Cologne (1995).

¹⁵ L. Arrachea, A. A. Aligia, E. Gagliano, K. Hallberg, and C. Balseiro, Phys. Rev. B **50**, 16044 (1994), (Erratum: B **52**, 9793 (1995)).

¹⁶ A. Aligia, K. Hallberg, C. Batista, and G. Ortiz, Phys. Rev. B **61**, 7883 (2000).

¹⁷ J. Appel, M. Grodzicki, and F. Paulsen, Phys. Rev. B **47**, 2812 (1993).

¹⁸ D. K. Campbell, J. T. Gammel, and E. Y. L. Jr., Phys. Rev. B **42**, 475 (1990).

¹⁹ A. A. Aligia and E. Gagliano, Phys. Rev. B **60**, 15332

(1999).

²⁰ C. Bourbonnais and D. Jérôme, in *Advances in Synthetic Metals, Twenty years of Progress in Science and Technology*, edited by P. Bernier, S. Lefrant, and G. Bidan (Elsevier, 1999), [cond-mat/0005111].

²¹ F. Dolcini and A. Montorsi, Phys. Rev. B **66**, 075112 (2002).

²² L. Arrachea and A. Aligia, Phys. Rev. Lett. **72**, 2240 (1994).

²³ A. Schadschneider, Phys. Rev. B **51**, 10386 (1995).

²⁴ J. de Boer, V. Korepin, and A. Schadschneider, Phys. Rev. Lett. **74**, 789 (1995).

²⁵ T. Nishino, J. Phys. Soc. Jpn. **64**, 3598 (1995).

²⁶ R. Bursill, T. Xiang, and G. Gehring, J. Phys.: Cond. Mat. **8**, L583 (1996).

²⁷ X. Wang and T. Xiang, Phys. Rev. B **56**, 5061 (1997).

²⁸ X. Wang and T. Xiang, *Density-Matrix Renormalization: A New Numerical Method in Physics* (Springer, 1999), vol. 528 of *Lecture Notes in Physics*, chap. 6, p. 149.

²⁹ H. F. Trotter, Proc. Am. Math. Soc. **10**, 545 (1959).

³⁰ M. Suzuki, Phys. Rev. B **31**, 2957 (1985).

³¹ A. Klümper, R. Raupach, and F. Schönfeld, Phys. Rev. B **59**, 3612 (1999).

³² J. Sirker and A. Klümper, Europhys. Lett. **60**, 262 (2002).

³³ J. Sirker and A. Klümper, Phys. Rev. B **66**, 245102 (2002).

³⁴ A. Kemper, A. Schadschneider, and J. Zittartz, J. Phys. A **34**, L279 (2001).

³⁵ A. Kemper, A. Gendiar, T. Nishino, A. Schadschneider, and J. Zittartz, J. Phys. A **36**, 29 (2003).

³⁶ C. Yang, Phys. Rev. Lett. **63**, 2144 (1989).

³⁷ C. Yang, Rev. Mod. Phys. **34**, 694 (1962).

³⁸ L. Arrachea, A. Aligia, and E. Gagliano, Phys. Rev. Lett. **76**, 4396 (1996).

- ³⁹ S. White, Phys. Rev. Lett. **69**, 2863 (1992).
- ⁴⁰ S. White, Phys. Rev. B **48**, 10345 (1993).
- ⁴¹ P. Jordan and E. Wigner, Z. Phys. **47**, 631 (1928).
- ⁴² H. Shiba, Phys. Rev. B **6**, 930 (1972).
- ⁴³ H. Schulz, Phys. Rev. Lett. **64**, 2831 (1990).
- ⁴⁴ G. Jüttner, A. Klümper, and J. Suzuki, Nucl. Phys. B **522**, 328 (1998).
- ⁴⁵ D. Vollhardt, Phys. Rev. Lett. **78**, 1307 (1997).
- ⁴⁶ N. Chandra, M. Kollar, and D. Vollhardt, Phys. Rev. B **59**, 10541 (1999).
- ⁴⁷ H. Shiba and M. Ogata, Prog. Theor. Phys. Suppl. **108**, 265 (1992).